2024 IEEE/RSJ International Conference on Intelligent Robots and Systems (IROS)
October 14-18, 2024. Abu Dhabi, UAE

Embedded 3D Printing of Silicone for Soft Actuator with Stiffness Gradient and Programmable Workspace

Fei Xiao[1,2], Zhuoheng Wei[1,2], Hao Wang[1,2], Jisen Li[1,2], Jian Zhu[1,2]

***Abstract* — Soft pneumatic actuators can accomplish various customizable deformation/motion through the distribution of cavities and gradients in stiffness. However, traditional manufacturing methods, say molding, struggle to produce soft actuators with both complex cavities and desirable stiffness distributions. Regular 3D printing methods usually need extra printheads for support materials to fabricate soft actuators with cavities. In addition, the printing quality and fidelity of the whole structure cannot be uniform due to the effect of gravity, especially for a soft actuator with overhang features. To fabricate a soft actuator of uniform fidelity but desirable stiffness distributions, we propose an embedded 3D printing approach with only one active mixing printhead. By adjusting the mixing ratio of the dual-component silicone, we can achieve desinated stiffness gradients, ranging from 30.2 kPa to 198 kPa. With this approach, we successfully fabricate soft pneumatic actuators with overhang features, which exhibit programmable elongation and radial expansion. Additionally, we fabricate soft bending actuators which can achieve programmable workspaces due to their predetermined stiffness distribution.**

I. Introduction

Soft robots, due to their inherent material compliance and safety, have wide-ranging applications in fields such as medical robotics, human-machine interaction, and delicate operations [1]. Among various types of soft robots, soft pneumatic actuators are widely utilized because of their unique affordability, excellent reversibility and controllability, as well as rapid actuation response [2].

The deformation of soft pneumatic actuators is usually achieved by morphological design of the internal cavities [3]. Their deformation can also be controlled by the stiffness distribution of materials, such as multimaterial design [4], reinforced skeleton [5], and wrapped fibers [6-8]. The inherent distributed compliance offered by freeform geometry and material diversity imbuing soft bodies with programmable mechanical properties to deliver desired complex deformation/motion. Therefore, it is significant to design and fabricate soft pneumatic actuators with complex cavities and stiffness distributions, in order to achieve desired behavior and functionality.

Traditional manufacturing methods of soft pneumatic actuators include soft lithography [9], lost wax casting [10], and rotational molding [11], etc. They usually involve intensive manual labor and complicated fabrication process. In addition, They are challenging to develop complex structures, which may consist of multiple cavities and multiple materials with different stiffnesses [12].

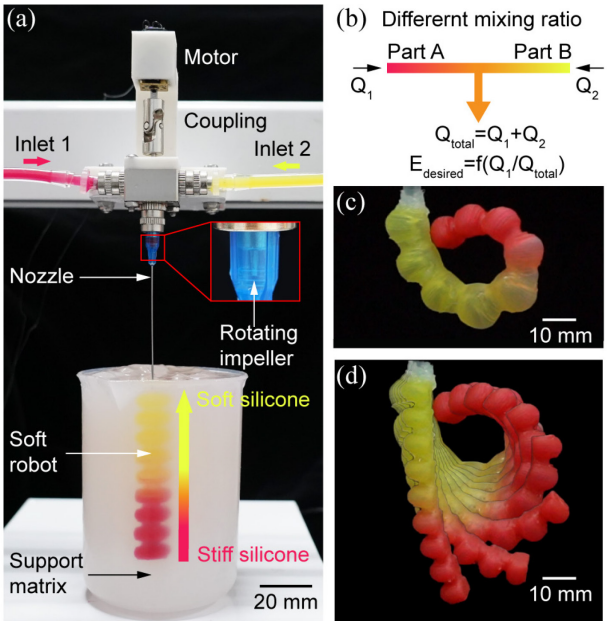

Fig. 1. Embedded 3d printing of silicone for soft actuator with stiffness gradient and programmable workspace. (a) Image of the embedded, active mixer 3D printer. (b) Schematic illustration of tuning the stiffness of the printed silicone by controlling the ratio of the flow rates of components A and B. (c) 3d printed soft actuators with stiffness gradient. (d) Programmable workspace of the 3d printed soft actuator.

With the advancement of 3D printing technology, many 3D printing techniques are being used to manufacture soft pneumatic actuators, including fused deposition modeling (FDM), digital light processing (DLP), inkjet, and direct ink writing (DIW) [13]. FDM typically uses thermoplastic polyurethane (TPU) materials, which are flexible but with limited stretchability [14]. In addition, FDM can only use a single material during the whole process of fabrication. DLP offers high resolution and are capable of printing intricate structures [15], while they are challenging to print multiple materials. Inkjet printing can fabricate soft actuators with high resolution [16] and multiple stiffnesses [17]. However, the mechanical properties, such as tensile strength, of the printed parts may not be robust [12].

Soft pneumatic actuators can be made of silicone and fabricated by the DIW method [18, 19]. The DIW technology can print soft pneumatic actuators with various stiffness distributions [20, 21]. However, they may require another printhead to print supporting materials, in order to fabricate a complex structure that consists of multiple chambers and/or cavities. In addition, due to the effect of gravity, the soft

[1]The authors are with School of Science and Engineering, The Chinese University of Hong Kong, 518172, Shenzhen, China (feixiao@link.cuhk.edu.cn; zhuohengwei@link.cuhk.edu.cn; haowang1@link.cuhk.edu.cn; lijisen@cuhk.edu.cn; zhujian@cuhk.edu.cn).
[2]The authors are with Shenzhen Institute of Artificial Intelligence and Robotics for Society, 518129, Shenzhen, China.
Corresponding author: Dr. Jian Zhu, zhujian@cuhk.edu.cn.

pneumatic actuator, fabricated by the regular DIW, may suffer a nonuniform quality and fidelity in the whole structure. Embedded 3D printing allows for fabricating freeform shapes without the need for support materials [22, 23]. In addition, due to the buoyancy force in the liquid environment, the whole body exhibits a limited effect of gravity and a uniform fidelity. Based on the embedded printing technique, a multi-nozzle printing system can fabricate a structure of multiple stiffnesses [24], but cannot achieve the stiffness gradient. Materials with stiffness gradients are capable of enhancing stress distribution at interfaces [25], demonstrating programmable deformation in soft actuators [1, 20, 21], and mimicking biological structures [26]. The printing method based on active mixing allows for the printing of materials with gradient properties by altering the mixing ratios [27-29]. For example, soft pneumatic robots with variable stiffness printing have been achieved by changing the silicone mixing ratio using static mixers, but it is difficult to achieve printing of complex structures [30, 31].

To print soft pneumatic actuators with complex structures and stiffness gradient distributions, we develop an embedded silicone 3D printing method with an active mixing printhead. The active mixing printhead incorporates a small mixing volume to facilitate rapid switching of proportions during printing. It employs dynamic stirring through a rotating impeller to ensure thorough mixing of the silicone. By adjusting the mixing ratio of the dual-component silicone, the stiffness of the silicone can be tuned accordingly. Combining an active mixing printhead with the embedded printing method enables the fabrication of structurally complex soft pneumatic actuators with stiffness gradient distributions. With this method, we 3D print a soft extending actuator with a specific stiffness gradient distribution, enabling programmable elongation and radial expansion. We also fabricate a soft bending actuator which can achieve a programmable workspace due to its predetermined stiffness distribution.

The main contributions of this work are summarized as follows.

- An active mixing printhead is designed with a small mixing volume to minimize dead zones and facilitate rapid switching of mixing ratio.
- Investigating the impact of silicone mixing ratio and slicing direction on the stiffness of silicone in embedded 3d printing.
- 3D printed a soft bending actuator that can achieve a programmable workspace due to its predetermined stiffness distributions.

II. EMBEDDED 3D PRINTING OF SILICONE

A. 3D Printer Setup

For this research, we design a custom embedded 3D printer. The printer primarily comprises a 3-axis gantry architecture, an active mixing printhead, a syringe pump (Fusion 4000, Chemyx), and a reservoir [see Fig. 1(a)]. The high-precision dual-channel syringe pump is employed to deliver the silicone materials (Part A and Part B) at a controlled flowrate into our active mixing printhead. The reservoir serves to hold the support matrix.

B. Extruder Mechanism

The active mixing printhead functions to blend the A and B components of silicone before introducing them into the support matrix. Positioned on either side of the active mixing printhead are the inlets for silicone Part A and Part B, distinguished by red and yellow staining agents. Upon entering the mixing chamber, the two silicone components are blended by the impeller and propelled downward by the pressure from the syringe pump. The impeller is driven by a 24V DC motor (200 RPM) and connected via a coupling. Connecting the mixing chamber to the dispense tips (22G precision, 0.41 mm ID, 38 mm long, Nordson EFD) is a Luer fitting. Through the dispense tips, the rotating impeller is visible [see Fig. 1(a)].

To enable rapid switching of mixing ratios during printing [27], the mixing chamber has an inner diameter of 2.75 mm and a length of 18 mm, while the impeller has a diameter of 2.1 mm and a length of 16 mm. Consequently, the total mixing volume is approximately 50 μL. For an extrusion needle with an inner diameter of 400 μm, a minimum of 397 mm of printed material is required to flush the mixer and switch to a new mixing ratio.

III. VARIABLE STIFFNESS 3D PRINTING

In this section, we outline the process of printing silicone samples using embedded 3D printing with various mixing ratios and subsequently conduct tensile tests to acquire their stress-strain curves. Concurrently, we will analyze the influence of different printing orientations on the sample stiffness.

Unlike DIW printing, in embedded printing, the mechanical properties of silicone are influenced by the support matrix because the support matrix is encapsulated within the silicone [22]. To examine the effect of the support matrix on silicone stiffness, we compare the stiffness of dogbone samples manufactured via embedded printing and direct ink writing (DIW), respectively.

Furthermore, we illustrate the discrete printing and continuous printing modes, showcasing our capability in 3D printing silicone with stiffness gradients.

A. Material

The printing material utilized is DragonSkin 10 Slow (Smooth-On), a 10-shore A silicone with a 1:1 mixing ratio. We supplemented both Part A and Part B with 2 wt % curing agent (SLO-JO, Smooth-on) and 3 wt % diluent (silicone thinner, Smooth-on). The addition of curing agent aims to extend the pot life, while the diluent is incorporated to lower viscosity and consequently reduce the required extrusion pressure. To differentiate the components and visualize the mixing ratio, we introduce red coloration to Part A and yellow coloration to Part B (Silc Pig, Smooth-On). Thorough mixing (2,000 rpm, 2 minutes) is achieved using a planetary mixer (ARV-310, Thinky).

The support matrix is prepared by thoroughly mixing silicone oil (silicone thinner, Smooth-On) and 3 wt % fumed-silica-based thickening agent (URE-FIL 9, Smooth-On) in a planetary mixer (2,000 rpm, 2 minutes). Reservoirs of different volumes are used to hold the support liquid to meet the requirements of printing size.

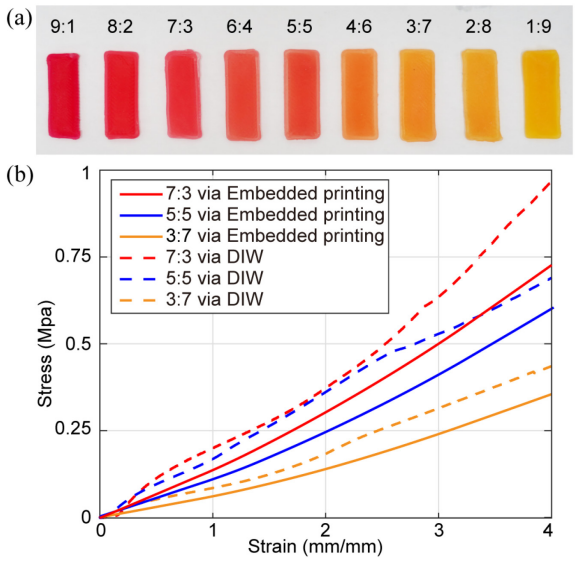

Fig. 2. (a) Embedded 3D printed samples with different mixing ratios. (b) Material properties of the samples based on the embedded and regular DIW printing techniques.

B. Mixing principle

This printing method achieves stiffness gradient printing by dynamically adjusting the mixing ratio of Part A and Part B during the printing process. As depicted in Fig. 1(b), this approach ensures a consistent total flow rate of silicone dispensed from the nozzle, thereby ensuring printing stability. The total flow rate is determined by the combined flow rates of Part A and Part B silicone entering the mixing chamber. By controlling the propulsion speed of the syringe pump, the flow rates of Part A and Part B can be adjusted, enabling precise control over the mixing ratio. We select a total flow rate of 10 ml/min.

C. Printing Process

The prepared silicone ink's part A and part B are loaded into two 10ml syringe barrels and centrifuged at 2,000 rpm for 4 min to remove any trapped air bubbles separately. The inks are then mounted to the syringe pump.

The generation of printing paths is carried out using slicing software (Simplify 3D). The print model is imported into the slicing software, where the print speed is adjusted to 5 mm/s, the print layer height to 400 µm, and the print infill density to 100%. The resulting Gcode file is then imported into a custom-made 3D printer to control the movement of the printer nozzle.

When printing the model, the nozzle deposits a specified mixing ratio of silicone along the printing path in the support matrix. After printing, the reservoir is placed inside a high-temperature oven at 80°C for 60 minutes to cure the printed silicone ink.

D. Results & Discussions

We print nine rectangular samples using nine different mixing ratios ranging from 9:1 to 1: 9, as depicted in Fig. 2(a). The color of the samples changes gradually from red to yellow from left to right. To investigate the impact of the support matrix on the stiffness of silicone. We also 3d print three types of dogbones via direct ink writing (DIW). As shown in Fig. 2(b), we mix Dragon Skin 10 Slow in ratios of 7:3, 5:5, and 3:7 respectively, and added a 3wt% thickening agent (Thi-Vex, Smooth-on). We then use a direct ink writing (DIW) printer to print three sets of dogbone (ASTM D412-C) samples. After curing, we conducted tensile tests using a Universal Testing Machine (AGS-X 500 N, Shimadzu) fitted with pneumatic grippers at a testing speed of 500 mm/min. to obtain stress-strain curves. It can be observed that, under all three mixing ratios, the samples printed directly with DIW exhibited higher stiffness compared to samples printed with embedded 3d printing. This indicates that embedded 3d printing reduces the stiffness of silicone. The softening effect could result from support matrix remnants trapped inside the structure.

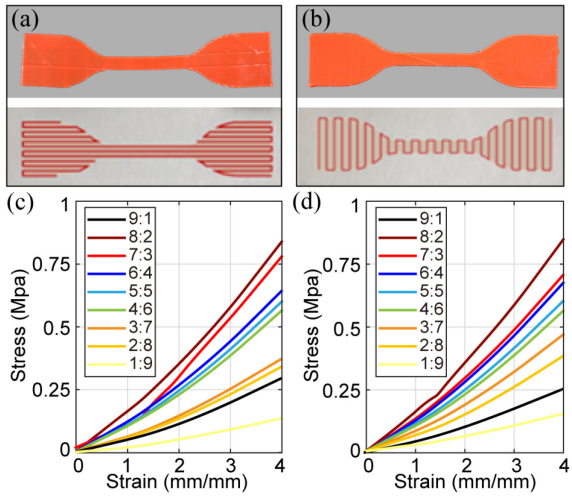

Fig. 3. Impact of infill direction and mixing ratio on silicone stiffness. (a, b) Dog bone samples printed with longitude and transverse infill directions respectively. (c, d) Stress-strain curves representing nine different mixing ratios for dog bone samples under longitude and transverse infill directions respectively.

In order to investigate the effect of silicone mixing ratios on stiffness in embedded printing, samples with different mixing ratios are also 3D printed in a dog bone shape for tensile testing. We conduct tensile testing on the samples. Stress-strain curves of samples of various proportions were obtained, as shown in Fig. 3.

In addition, to investigate whether the silicone printed in horizontal and vertical orientations exhibited similar strength, dogbone models with different infill orientations were 3D printed and subjected to tensile tests. Fig. 3(a) and (b) depict the samples with longitudinal and transverse infill orientations, respectively. Fig. 3(c) and (d) illustrate the stress-strain curves of the samples with longitudinal and transverse infill orientations, respectively. Under embedded 3d printing methods, it's evident that silicone maintains high elongation rates in both horizontal and vertical orientations, exceeding 400%. This level of elongation is sufficient for driving soft pneumatic soft robots.

From the data, we determine the stiffness of the samples by calculating Young's modulus value E of the material at 100% of its initial length.

As depicted in Fig. 4, the stiffness of the silicone increases from 30.2 kPa to 198 kPa with the rise in the proportion of Part A. However, once the Part A proportion surpasses 90%,

curing the silicone becomes challenging, resulting in a highly viscous surface. Consequently, we choose to print silicone with Part A proportions ranging from 10% to 80%. Interestingly, both printing orientations showcase similar stiffness across different ratios, indicating a minimal correlation between printing orientation and sample stiffness. This suggests that silicone printed in both horizontal and vertical orientations exhibits comparable strength.

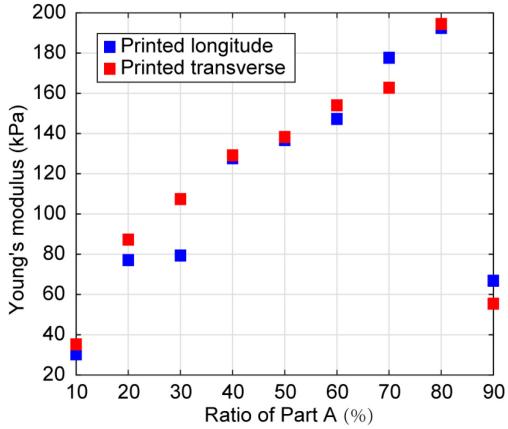

Fig. 4. Young's modulus as a function of the ratio of Part A

Two Printing Mode

In this section, we demonstrate two printing modes: discrete mode and continuous mode. The discrete mode prints a finite number of stiffnesses during model printing, as shown in Fig. 5. In printing, when a change in stiffness is required, purging the previous ratio of material is necessary using a wipe tower before continuing with the printing process. This results in material and time wastage.

In Fig. 5(a), we print rectangles using a discrete mode with A-component ratios of 60% (red) and 40% (yellow) respectively. During printing, we start with a 60% mixture ratio, and when it is necessary to switch ratios, the remaining material in the mixing chamber is purged before proceeding with the 40% ratio printing. By stretching the rectangle, the red portion exhibits a smaller elongation compared to the yellow portion, indicating a discrete distribution of stiffness.

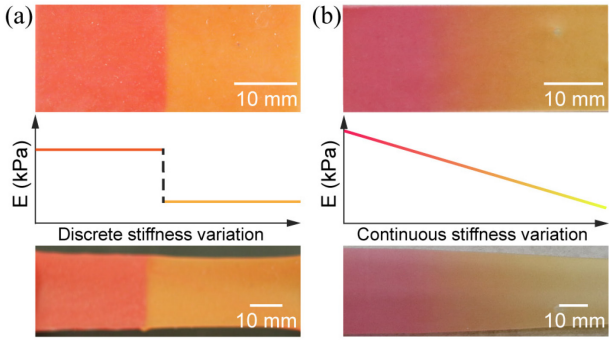

Fig. 5. Two printing modes. (a) Discrete mode, stepwise graded structure. (b) Continuous mode with stiffness gradient.

In Fig. 5(b), we also print a rectangle using continuous mode, printing from left to right. At the beginning of printing, the A-component ratio is 80%, and at the end of printing, the A-component ratio is 30%. It can be observed that during the printing process, the color transitions continuously from red to yellow. Upon stretching this specimen, the elongation gradually increases from left to right, demonstrating a continuously decreasing stiffness distribution in the rectangle.

Printing in continuous mode requires careful attention to the speed of switching mixing ratios since there is no purging of waste material. We conduct speed tests for ratio switching using the active mixing printhead. We print a rectangular piece from left to right, with the mixing ratio alternating between 60% and 40% every 90 seconds (see Fig. 6). The resulting sample shows clear distinctions between the red and yellow regions, with dashed yellow lines added to denote the regions of different mixing ratios. The rapid ratio switching is facilitated by designing a mixing chamber with minimal volume.

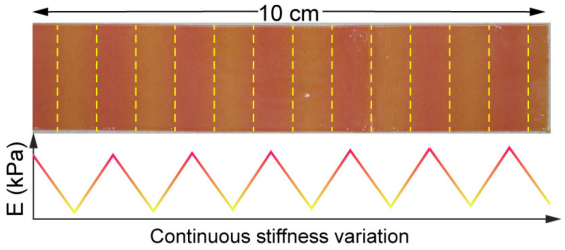

Fig. 6. Active mixing printhead achieves fast switching of mixing ratio, dashed yellow lines added to denote the boundaries of regions with different mixing ratios.

IV. APPLICATIONS

In this section, we demonstrate two types of soft pneumatic actuators to prove our ability to print overhang structures with gradient stiffness distributions: soft extending actuators and soft bending actuators. By adjusting the stiffness distributions, the pneumatic soft actuators can exhibit programmable motion.

A. Soft Extending Actuators

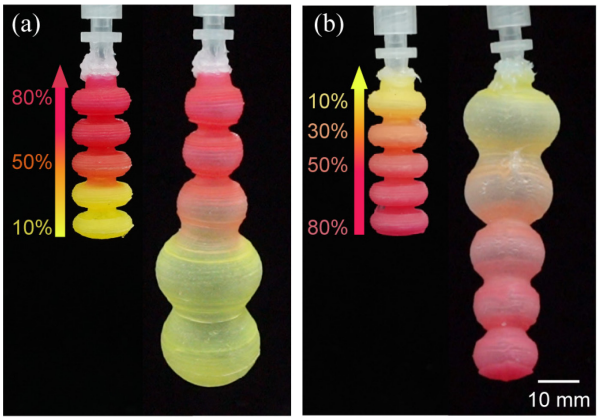

Fig. 7. Soft extending actuators with different stiffness gradients.

The initial demonstration features a soft extending actuator, as shown in Fig. 7. This actuator is a type of bellowed soft actuator with a total length of 36 mm and a radius of a single bellow of 2 mm. The maximum diameter of the actuator is 14 mm. It consists of a total of 5 bellows, each with a wall thickness of 0.4 mm. The printing time required for this actuator is 11 minutes. Typically, this type of actuator requires support material when using alternative printing methods, making it more challenging to print.

The actuator's varying colors represent different stiffness levels. From bottom to top, there is a transition from yellow to orange to red, corresponding to mass proportions of 10%, 50%, and 80% of silicone Part A, respectively. Stiffness also increases with the proportion of component A [see Fig. 7 (a)]. Upon inflation with a pressure of 8 kPa, the actuator expands and elongates. Deformation varies across different stiffness regions, with the yellow part exhibiting greater elongation and radial expansion, the red area showing smaller deformation, and the middle region demonstrating a gradient change in deformation. The radial expansion rate of the yellow part reaches 186%, while the actuator's elongation rate reaches 194%.

The motion of the actuator can be programmed, and different stiffness levels can be specified for different areas of the actuator, as depicted in Fig. 7(b). In this configuration, the stiffness gradient is set in the opposite direction, with a specified silicone component A content of 30% added. Consequently, when driven by air pressure, this actuator exhibits radial expansion opposite to that of the actuator in Fig. 7(a).

B. Soft Bending Actuators

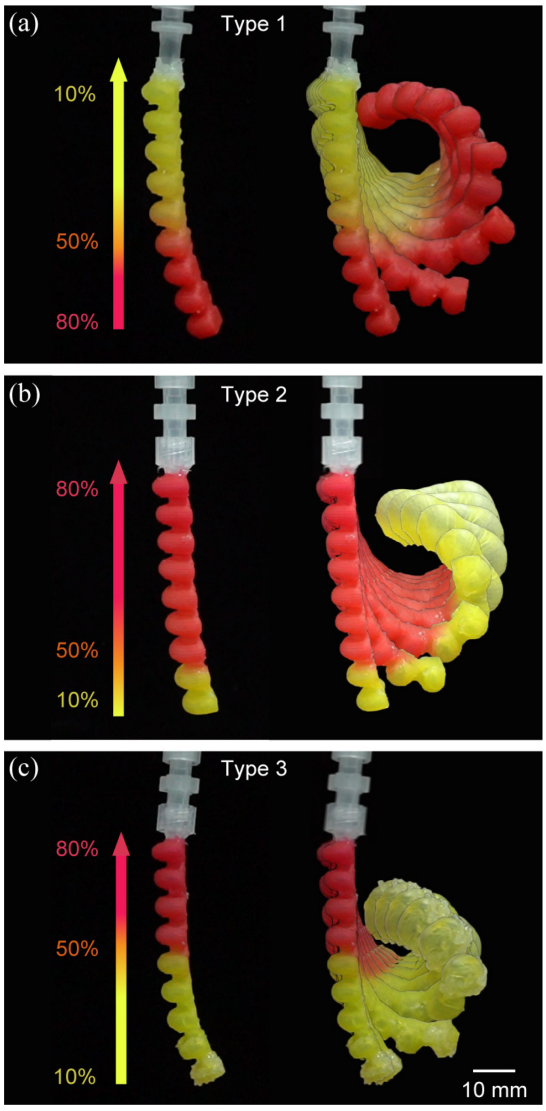

Fig. 8. Soft bending actuators with programmable workspace.

The second demonstration involves the printing of soft bending actuators. These actuators have a length of 6 cm, a radius of 6 mm, a wall thickness of 0.4 mm, and a total of 9 chambers. The printing time required is 17 minutes. Three bending actuators with varying stiffness gradient distributions were printed, as illustrated in Fig. 8.

In the first type bending actuator, stiffness decreases from bottom to top. The first three chambers contain 80% of Part A, while the fourth transitions from 80% to 50%, and the fifth transitions from 50% to 10%. Consequently, the actuator's stiffness decreases from bottom to top. The bending angle of the actuator is recorded and monitored throughout the experiment. As shown in Fig. 9(a), results reveal that by increasing the pressure, the bending angle is also increased. Under 8 kPa pressure, its maximum bending angle is 290°. With lower stiffness at the root and higher stiffness at the end, the root exhibits a larger bending angle, as depicted in Fig. 8(a).

For the second type actuator, the region with low stiffness is confined to a small range at the end. Consequently, the actuator achieves a large bending angle within this limited range. As a result, the workspace is smaller than type 1. Under 8 kPa pressure, the maximum bending angle of the actuator is 310°, as depicted in Fig. 8(b) and Fig. 9(a).

In type 3, the area with low stiffness extends over a larger range at the end, enabling a larger total bending angle to be achieved. Under 8 kPa pressure, the maximum bending angle of the actuator is 319°, as illustrated in Fig. 8(c) and Fig. 9(a).

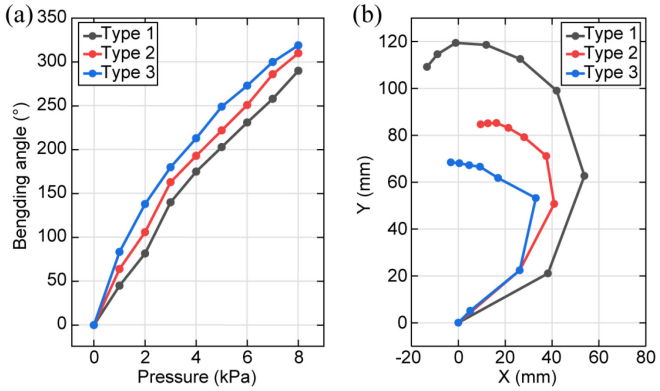

Fig. 9. (a) The bending angle at different supply pressures for three types of soft bending actuators, and (b) a comparison of their workspaces.

By tracking the trajectories of the endpoints of the three soft bending actuators with different stiffness distributions, we obtained the endpoint trajectories of the three actuators under pressure driving and plotted their workspace, as shown in Fig. 9(b). It can be observed that Type 1 has the largest workspace, while Type 3 has the smallest workspace. The difference in Y-axis movement space between these two types is nearly twice as much. This indicates that we can achieve programmable deformation by programming the stiffness distribution of soft bending actuators.

V. Conclusion

To manufacture soft pneumatic actuators with intricate shapes and stiffness gradient distributions, we've devised an embedded 3D printing approach with only one active mixing

printhead. This printhead integrates a compact mixing volume, enabling swift switching of proportions during printing. Utilizing dynamic stirring via a rotating impeller ensures thorough mixing of the silicone. Employing a single dual-component silicone during printing allows for real-time adjustment of stiffness by modifying the mixing ratio. The combination of the active mixing printhead with embedded printing techniques enables the production of complex soft pneumatic actuators with gradient stiffness distributions. This approach facilitates the 3D printing of a soft extending actuator with programmable elongation and radial expansion. Furthermore, we created soft bending actuators, enabling robots to have customizable workspaces by implementing programmable stiffness distributions.

Future work will explore developing 3D printed soft actuators with bioinspired structures. These structures will have programmable stiffness distribution, allowing them to perform intricate movements such as twisting, conformal bending, and coupled motions.

ACKNOWLEDGMENT

J.L. acknowledges the support from the National Natural Science Foundation of China under Grant No. 52105034. J.Z. acknowledges the Funding of Shenzhen City (2023 SZSTI stable support scheme for universities), the Funding of Shenzhen Institute of Artificial Intelligence and Robotics for Society (AC01202101113), the Funding of Guangdong Province (2021CX02Z251) and the Funding of China Merchants Group (BN00202312037).

REFERENCES

[1] D. Rus and M. T. Tolley, "Design, fabrication and control of soft robots," *Nature,* vol. 521, no. 7553, pp. 467-475, 2015/05/01 2015.

[2] G. M. Whitesides, "Soft Robotics," *Angewandte Chemie International Edition,* vol. 57, no. 16, pp. 4258-4273, 2018/04/09 2018.

[3] F. Chen, Z. Song, S. Chen, G. Gu, and X. Zhu, "Morphological Design for Pneumatic Soft Actuators and Robots With Desired Deformation Behavior," *IEEE Transactions on Robotics,* 2023.

[4] L.-K. Ma, Y. Zhang, Y. Liu, K. Zhou, and X. Tong, "Computational design and fabrication of soft pneumatic objects with desired deformations," *ACM Trans. Graph.,* vol. 36, no. 6, p. Article 239, 2017.

[5] S. Chen *et al.*, "Topology Optimization of Skeleton-Reinforced Soft Pneumatic Actuators for Desired Motions," *IEEE/ASME Transactions on Mechatronics,* vol. 26, no. 4, pp. 1745-1753, 2021.

[6] F. Connolly, C. J. Walsh, and K. Bertoldi, "Automatic design of fiber-reinforced soft actuators for trajectory matching," *Proceedings of the National Academy of Sciences,* vol. 114, no. 1, pp. 51-56, 2017.

[7] P. Polygerinos *et al.*, "Modeling of soft fiber-reinforced bending actuators," *IEEE Transactions on Robotics,* vol. 31, no. 3, pp. 778-789, 2015.

[8] F. Connolly, P. Polygerinos, C. J. Walsh, and K. Bertoldi, "Mechanical programming of soft actuators by varying fiber angle," *Soft Robotics,* vol. 2, no. 1, pp. 26-32, 2015.

[9] B. Mosadegh *et al.*, "Pneumatic networks for soft robotics that actuate rapidly," *Advanced functional materials,* vol. 24, no. 15, pp. 2163-2170, 2014.

[10] A. D. Marchese, R. K. Katzschmann, and D. Rus, "A recipe for soft fluidic elastomer robots," *Soft robotics,* vol. 2, no. 1, pp. 7-25, 2015.

[11] H. Zhao, Y. Li, A. Elsamadisi, and R. Shepherd, "Scalable manufacturing of high force wearable soft actuators," *Extreme Mechanics Letters,* vol. 3, pp. 89-104, 2015.

[12] D. Wang *et al.*, "Soft actuators and robots enabled by additive manufacturing," *Annual Review of Control, Robotics, and Autonomous Systems,* vol. 6, pp. 31-63, 2023.

[13] T. Wallin, J. Pikul, and R. F. Shepherd, "3D printing of soft robotic systems," *Nature Reviews Materials,* vol. 3, no. 6, pp. 84-100, 2018.

[14] H. K. Yap, H. Y. Ng, and C.-H. Yeow, "High-force soft printable pneumatics for soft robotic applications," *Soft Robotics,* vol. 3, no. 3, pp. 144-158, 2016.

[15] D. K. Patel, A. H. Sakhaei, M. Layani, B. Zhang, Q. Ge, and S. Magdassi, "Highly stretchable and UV curable elastomers for digital light processing based 3D printing," *Advanced Materials,* vol. 29, no. 15, p. 1606000, 2017.

[16] R. MacCurdy, R. Katzschmann, K. Youbin, and D. Rus, "Printable hydraulics: A method for fabricating robots by 3D co-printing solids and liquids," in *2016 IEEE International Conference on Robotics and Automation (ICRA)*, 16-21 May 2016 2016, pp. 3878-3885, doi: 10.1109/ICRA.2016.7487576.

[17] X. Sheng, H. Xu, N. Zhang, N. Ding, X. Zhu, and G. Gu, "Multi-material 3D printing of caterpillar-inspired soft crawling robots with the pneumatically bellow-type body and anisotropic friction feet," *Sensors and Actuators A: Physical,* vol. 316, p. 112398, 2020.

[18] J. Plott and A. Shih, "The extrusion-based additive manufacturing of moisture-cured silicone elastomer with minimal void for pneumatic actuators," *Additive Manufacturing,* vol. 17, pp. 1-14, 2017.

[19] O. D. Yirmibesoglu *et al.*, "Direct 3D printing of silicone elastomer soft robots and their performance comparison with molded counterparts," in *2018 IEEE international conference on soft robotics (RoboSoft)*, 2018: IEEE, pp. 295-302.

[20] M. Schaffner, J. A. Faber, L. Pianegonda, P. A. Rühs, F. Coulter, and A. R. Studart, "3D printing of robotic soft actuators with programmable bioinspired architectures," *Nature communications,* vol. 9, no. 1, p. 878, 2018.

[21] M. A. Skylar-Scott, J. Mueller, C. W. Visser, and J. A. Lewis, "Voxelated soft matter via multimaterial multinozzle 3D printing," *Nature,* vol. 575, no. 7782, pp. 330-335, 2019/11/01 2019.

[22] T. E. Greenwood, S. E. Hatch, M. B. Colton, and S. L. Thomson, "3D printing low-stiffness silicone within a curable support matrix," *Additive manufacturing,* vol. 37, p. 101681, 2021.

[23] S. Duraivel *et al.*, "A silicone-based support material eliminates interfacial instabilities in 3D silicone printing," *Science,* vol. 379, no. 6638, pp. 1248-1252, 2023.

[24] Z. Wang *et al.*, "Multimaterial Embedded 3D Printing of Composite Reinforced Soft Actuators," *Research,* vol. 6, p. 0122, 2023.

[25] A. Miserez, T. Schneberk, C. Sun, F. W. Zok, and J. H. Waite, "The transition from stiff to compliant materials in squid beaks," *Science,* vol. 319, no. 5871, pp. 1816-1819, 2008.

[26] Z. Liu, M. A. Meyers, Z. Zhang, and R. O. Ritchie, "Functional gradients and heterogeneities in biological materials: Design principles, functions, and bioinspired applications," *Progress in Materials Science,* vol. 88, pp. 467-498, 2017.

[27] T. J. Ober, D. Foresti, and J. A. Lewis, "Active mixing of complex fluids at the microscale," *Proceedings of the National Academy of Sciences,* vol. 112, no. 40, pp. 12293-12298, 2015.

[28] P. A. G. S. Giachini *et al.*, "Additive manufacturing of cellulose-based materials with continuous, multidirectional stiffness gradients," *Science Advances,* vol. 6, no. 8, p. eaay0929.

[29] C. A. Young, M. O'Bannon, and S. L. Thomson, "Three-Dimensional Printing of Ultrasoft Silicone with a Functional Stiffness Gradient," *3D Printing and Additive Manufacturing,* vol. 11, no. 2, pp. 435-445, 2024/04/01 2022.

[30] B. Parilusyan, A.-E. Nicolae, T. Batigne, C. Duhart, and M. Serrano, "Bi-Component Silicone 3D Printing with Dynamic Mix Ratio Modification for Soft Robotic Actuators," in *2023 IEEE/RSJ International Conference on Intelligent Robots and Systems (IROS)*, 2023: IEEE, pp. 8237-8242.

[31] Z. Jiao, Z. Zhuang, L. Hu, C. Sun, Y. Yu, and W. Yang, "Hardness and modulus programmable tuning for silicone 3D printing device and experiment," *Rapid Prototyping Journal,* vol. 29, no. 7, pp. 1536-1545, 2023.